European Journal of Pharmaceutics and Biopharmaceutics 75 (2010) 96–106

Contents lists available at ScienceDirect

European Journal of Pharmaceutics and Biopharmaceutics

journal homepage: www.elsevier.com/locate/ejpb

Research paper

Effect of polyethylene glycol (PEG) chain organization on the physicochemical properties of poly(D, L-lactide) (PLA) based nanoparticles

Sherief Essa, Jean Michel Rabanel, Patrice Hildgen *

Department of Pharmaceutical Technology, Monteral University, Québec, Canada

ARTICLE INFO

Article history:
Received 19 October 2009
Accepted in revised form 1 March 2010
Available online 6 March 2010

Keywords:
Poly(D, L-lactide)
Polymer architecture
Graft polymers
Multiblock
Chain organization
X-ray photoelectron spectroscopy (XPS)

ABSTRACT

The aim of the present study is to evaluate the effect of polyethylene glycol (PEG) chain organization on various physicochemical aspects of drug delivery from poly(D, L-lactide) (PLA) based nanoparticles (NPs). To reach that goal, two different pegylated polymers of poly(D, L-lactide) (PLA) were synthesized. Polymers used in this study are grafted ones in which PEG was grafted on PLA backbone at 7% (mol/mol of lactic acid monomer), PEG7%-g-PLA, and multiblock copolymer of both PLA and PEG, (PLA–PEG–PLA)*n* with nearly similar PEG insertion ratio and the same PEG chain length. Blank and ibuprofen-loaded NPs were prepared from both polymers and their properties were compared to PLA homopolymer NPs as a control. Encapsulation efficiency of ibuprofen was found to be ~25% for (PLA–PEG–PLA)*n* NPs and ~80% for PEG7%-g-PLA NPs. (PLA–PEG–PLA)*n* NPs either blank or loaded showed larger hydrodynamic diameter (~200 nm) than PEG7%-g-PLA NPs (~135 nm). A significant difference was observed in the amount of PVA associated with the surface of both NPs where 3.6% and 0.4% (wt/wt) were found on the surface of PEG7%-g-PLA and (PLA–PEG–PLA)*n* NPs, respectively. No observed difference in zeta potential values for both NPs formulations was found. DSC showed the existence of the drug in a crystalline state inside NPs matrix irrespective of the type of polymer used with either shifting or/ and broadening of the drug melting endotherm. Both AFM phase imaging and XPS studies revealed the possibility of existence of more PEG chains at the surface of grafted polymer NPs than (PLA–PEG–PLA)*n* during NPs formation. The in vitro release behavior showed that (PLA–PEG–PLA)*n* NPs exhibited faster release rates than PEG7%-g-PLA NPs. The physicochemical differences obtained between both polymers were probably due to different chain organization during NPs formulation. Such pegylated NPs made from these two different polymers might find many applications, being able to convert poorly soluble, poorly absorbed substances into promising drugs, improving their therapeutic performance, and helping them reach adequately their target area. Our results suggest that the properties of pegylated PLA-based NPs can be tuned by proper selection of both polymer composition and polymer architecture.

1. Introduction

Over the past few decades, there has been an intensive research on the development of biodegradable nanoparticles (NPs) as a suitable means for controlled drug release and targeting [1–3] Nanoparticles (NPs) are colloidal systems that vary in size from 10 to 1000 nm. The drug is either dissolved, entrapped, encapsulated, or attached to a nanoparticle matrix [4]. Poly(lactic acid) (PLA) or poly(lactide-co-glycolide) (PLGA) has been widely used to fabricate NPs owing to excellent biocompatibility, biodegradability and high encapsulation capability for hydrophobic drugs. However, uptake of such naked NPs by the reticuloendothelial system after intravascular administration presented a major problem for achieving effective targeting to specific sites in the body other than liver and spleen [5]. Therefore, the design of long-circulating NPs or stealth NPs has emerged as an attempt to escape recognition by phagocytic cells of the blood. The most commonly used strategy for designing stealth NPs is reliant upon introducing flexible hydrophilic coat onto hydrophobic surfaces, shielding them against plasma protein adsorption, which is the first step of particle clearance mechanism by blood phagocytes. Covalently grafted PEG strategy was proven stable and more successful than physical adsorption of PEG containing surfactants onto NPs surface. Generally, covalent copolymers of PLA (A) and PEG (B) can be divided into single-sided grafted defined as grafted or diblock copolymer (A–B) and double-sided grafted denoted as triblock copolymer (A–B–A) or multiblock copolymer (A–B–A)*n*. Many attempts have been made in the past to fabricate NPs using diblock copolymers of either PLA–PEG or PLGA–PEG [3,6]. Up to now, however, relatively fewer studies have focused on grafted pegylated and

* Corresponding author. C.P. 6128, Succursale Centre-Ville, Montréal, Québec, Canada H3C 3J7. Tel.: +1 (514) 343 6448; fax: +1 (514) 343 6871.
E-mail address: Patrice.hildgen@umontreal.ca (P. Hildgen).

0939-6411/$ - see front matter © 2010 Elsevier B.V. All rights reserved.
doi:10.1016/j.ejpb.2010.03.002

multiblock copolymers of PLA and PEG. In this study, we are hypothesizing that it is difficult for hydrophilic PEG domains of multiblock copolymer NPs to move freely towards NPs surface as PEG-g-PLA NPs. The major objective of this study was first to optimize NPs formulation using two pegylated polymers of different PEG chain organization, one is grafted, PEG7%-g-PLA and the second is multiblock copolymer of PLA and PEG, (PLA–PEG–PLA)*n*. Second, to study the effect of PEG chain organization on the physicochemical properties of the obtained NPs. Poly(lactic acid) (PLA) homopolymer was proposed as the hydrophobic control in our study. Ibuprofen was used as a model lipophilic drug to be encapsulated by PLA- and PEG-modified PLA NPs. NPs were formulated using emulsion–solvent evaporation method and poly(vinyl alcohol) (PVA) was mainly used as an emulsifier to stabilize the emulsion droplets since it aids the formation of relatively small sized particles with uniform size distribution [7].

2. Material and methods

2.1. Materials

D, L-Dilactide, poly(ethylene glycol) methyl ether (MePEG; 2000 Da), poly(ethylene glycol) (PEG, 1500 Da), allyl glycidyl ether, tetraphenyltin, polyvinyl alcohol (PVA, average M_w 9000–10,000 Da, 80% hydrolyzed), succinic acid, 1-ethyl-3-[3-dimethylaminopropyl]-carbodiimide (EDC), 4-dimethylaminopyridine (4-DMAP), pyridine, acetone, chloroform, diethyl ether, and N,N-dimethylformamide were purchased from Aldrich Chemical Company Inc., Milwaukee, USA. Ibuprofen was obtained from Medisca Pharmaceutical Inc., Montreal, Quebec, Canada. Sodium hydroxide pellets were purchased from Anachemia Canada Inc., and dichloromethane (DCM) was purchased from Laboratoire Mat Inc., Montreal, Quebec, Canada.

2.2. Synthesis of polymers

The homopolymer poly(D, L)-lactide (PLA) was synthesized by ring-opening polymerization of dilactide in argon atmosphere, using tetraphenyltin as the catalyst. Bulk polymerization was carried at 180 °C for 6 h in a round-bottom flask and purged thoroughly with argon. The obtained polymer was dissolved in acetone and then purified by precipitating in water.

Polymer with poly(ethylene glycol)-grafted randomly on poly (D, L)-lactide at 7% grafting density, PEG7%-g-PLA (PEG; M_w 2000 Da) was synthesized in the laboratory as reported earlier by our group [8]. Multiblock copolymer, (PLA–PEG–PLA)*n* was also synthesized as previously reported [9] using PEG with M_n of 1500 and succinic acid was used as condensing agent to link triblock copolymers. (PLA–PEG–PLA)*n* was synthesized to yield a PEG (1500)/lactic acid monomer ratio of 7% (mol/mol). ^{1}H NMR spectra were recorded on a Brucker ARX 400 spectrometer (Bruker Biospin, Billerica, MA). Chemical shifts (δ) were measured in parts per million (ppm) using tetramethylsilane (TMS) as an internal reference. Gel permeation chromatography (GPC) was performed on a Water Associate chromatography system (Waters, Milford, MA) equipped with a refractive index detector and a Phenomenex Phenogel 5-μ column. Polystyrene standards were used for calibration with THF as the mobile phase at a flow rate of 0.6 mL/min.

2.3. Preparation of nanoparticles (NPs)

NPs were prepared by an (O/W) emulsion–solvent evaporation method. It should be mentioned that NPs could not be prepared using the multiblock copolymer alone due to its low molecular weight as revealed by GPC data (Table 1); hence, a 1:1 mixture of PLA and multiblock copolymer was used for the preparation of NPs. For blank NPs, each polymer or polymer blend in case of multiblock (1 g) was dissolved in 35 mL DCM and emulsified in 100 mL PVA solution (0.5% w/v) as an external aqueous phase using high-pressure homogenizer (Emulsiflex C30, Avestin, Ottawa, Canada) at a pressure of 10,000 psi for 5 min. The emulsion was collected by washing with another 100 mL of 0.5% PVA. The DCM was evaporated under reduced pressure with constant stirring to obtain the NPs. Finally, NPs obtained as a suspension were then collected by centrifugation at 41.340 g for 1 h at 4 °C (Sorval® Evolution$_{RC}$, Kendro, USA), washed four times with distilled water, then lyophilized in the presence of 5% w/v sucrose as a cryoprotectant to obtain dry NPs (Freeze Dry System, Lyph.Lock 4.5, Labconco) and stored at 4 °C until further use. Ibuprofen-loaded NPs were prepared in a similar manner to that of blank NPs using initial loading of 10% wt/wt of each polymer. Ibuprofen was first dissolved in the organic phase followed by dissolution of the polymer. The emulsification and purification steps procedure were repeated as before.

2.4. Characterization of NPs

2.4.1. Particle size and size distribution

Particle size and size distribution of NPs were measured by dynamic light scattering (DLS) with a Malvern Autosizer 4800 instrument (Malvern Instruments, Worcestershire, UK) before and after lyophilization. For all batches, fresh NP suspensions (0.1 mL) or lyophilized NPs (1 mg) were diluted 10 times with Milli-Q Water, and size measurements were performed at 25 °C and scattering angle of 90°. The CONTIN program was used to extract size distributions from the autocorrelation functions. Measurements were performed in triplicate.

2.4.2. NPs surface morphology and phase image analysis

Surface morphology and phase imaging of NPs were studied using Nanoscope IIIa Dimension 3100 atomic force microscope (Digital Instruments, Santa Barbara, CA, USA). Samples were prepared by deposition of particle suspension in Milli-Q Water on freshly cleaved mica followed by air-drying. Topography and phase images of these samples were captured simultaneously using TappingMode™ etched silicon probes (TESP7) with tip radius of 5–10 nm, spring constant of 20–100 N/m and resonance frequency

Table 1
Polymers characterization by ^{1}H NMR, DSC, and gel permeation chromatography (GPC).

Polymer	M_n[a]	M_w[a]	M_w/M_n[a]	PEG insertion (mol%)[b]	M_n (^{1}H NMR)[b]	T_g (°C)[c]
PLA	40,318	56,171	1.4	N/A	N/A	46.4
PEG7%-g-PLA	3752	8392	2.2	4.1%	8336	53
(PLA–PEG–PLA)*n*	3508	3982	1.2	8.9%	3780	39

N/A: Not analyzed.
[a] Determined by GPC analysis using narrow molecular weight polystyrene standards. M_w/M_n = Polydispersity index of the polymers (PDI).
[b] Calculated from peak intensity ratios of PEG (3.6 ppm) and PLA (5.2 ppm) by ^{1}H NMR.
[c] Calculated from the second run of DSC as half of the extrapolated tangents in case of PLA and (PLA–PEG–PLA)*n* or as an endothermic peak in case of PEG7%-g-PLA.

of 200–500 kHz. Cantilever length was 125 μm. A set-point ratio (rsp, ratio of engaged oscillation amplitude to free air oscillation amplitude) between 0.5 and 0.7 (moderate tapping mode) was used for all topographic and phase images unless otherwise stated.

2.4.3. Zeta (ζ) potential measurements

NPs were suspended in 0.22 μm filtered 0.25% (w/v) saline solution, and ζ-potential was measured on Malvern ZetaSizer Nanoseries ZS (Malvern Instruments, Worcestershire, UK) in triplicate.

2.4.4. Encapsulation efficiency (EE)

A weighed amount of NPs was digested in 1 N NaOH for 1 h. Ibuprofen concentration was measured by spectrophotometry at 264 nm (U-2001 UV/Visible spectrophotometer, Hitachi). Percent encapsulation efficiency (% EE) and % drug loading (% DL) were calculated based on the following equations:

$$\%EE = \frac{\text{Amount of drug entrapped in NPs}}{\text{Initial amount of drug added}} \times 100 \quad (1)$$

$$\%DL = \frac{\text{Amount of drug entrapped in NPs}}{\text{Initial amount of drug added}} \times 100 \quad (2)$$

2.4.5. Determination of residual PVA

The amount of PVA remaining in the NPs was determined by a colorimetric method based on the formation of a colored complex between two adjacent hydroxyl groups of PVA and an iodine molecule [7]. First, to determine the surface-associated PVA, certain weight of NPs was suspended in distilled water followed by vigorous vortexing for 10 min, then fixed volumes of all formulations were withdrawn followed by the addition of 5 mL of saturated solution of boric acid and 0.5 mL iodine (0.1 N), and the volume was made up to 10 mL with distilled water. The absorbance of the formed complex was measured at 660 nm against similarly treated blank. Whereas for the total amount of PVA associated with the particles (amount entrapped inside the matrix as well as present on the surface), NPs were digested in 1 N NaOH then neutralized by 1 N HCl followed by stirring for 1 h and the volume was made up to 5 mL with distilled water. To this, 3 mL of saturated solution of boric acid and 0.5 mL iodine (0.1 N) were added, and the volume was made up to 10 mL with distilled water. The absorbance was measured as earlier. The amount of PVA was calculated by using the calibration curve of PVA prepared under the same conditions.

2.4.6. Differential Scanning Calorimetry (DSC)

The thermal properties of the pure polymers, physical mixtures of ibuprofen with each polymer, and NPs were characterized by DSC analysis (DSC 30, Mettler TA 4000, Schwerzenbach, Switzerland) with refrigerated cooling. The purge gas was purified nitrogen at a pressure of 20 psi. For pure polymers, weighed samples were sealed in crimped aluminum pans with lids using an empty pan as a reference and were heated at a rate of 10 °C/min from −50 to 200 °C (two runs), while for NPs the samples were heated from −50 to 90 °C(two runs) at the same heating rate.

2.4.7. XPS analysis

Surface chemistry of pure materials, polymers, blank, and drug-loaded NPs was characterized by X-ray photoelectron spectroscopy (VG Scientific ESCALAB MK II) with a monochromatized Mg Ka X-rays (hv 1253.6 eV) and an electron take off angle of 0°. A single survey scan spectrum (0–1000 eV) and narrow scans for C1s (210–305 eV) and O1s (525–550 eV) were recorded for each sample with a pass energy of 1 and 0.5 eV, respectively. Acquisition and data analysis were performed by a VGS 5000 data system. Peak fitting of the C1s envelope was as described by Shakesheff et al. [10].

2.4.8. 1H NMR spectroscopy

A weighed amount of nanoparticles lyophilized in presence of sucrose (50 mg) was suspended in 10 mL distilled water and centrifuged (5000 rpm, 10 min). The residues were washed three times with water to remove sucrose (cryoprotectant) that might show any interference during ^{1}H NMR analysis of NPs. Then, NPs were lyophilized for 24 h. Relyophilized NPs were suspended in deuterium oxide (D_2O). ^{1}H NMR spectra were recorded on the same machine used before for analysis of synthesized polymers.

2.4.9. Erosion study

Erosion (mass loss) studies of (A) PLA, (B) PEG7%-g-PLA, and (C) (PLA–PEG–PLA)*n* NPs were done by suspending 50 mg of NPs for each time interval in 10 mL PBS, pH 7.4 at 37 °C in shaking water bath. The study was terminated at 0, 5, 14, 25, 35, and 45 days. Samples were centrifuged (5000 rpm, 10 min) at the end of each time interval. The residues were washed two times with water to remove phosphate buffer and lyophilized for 24 h. The final mass of NPs was determined at each time point.

2.4.10. In vitro drug release study

Loaded formulations prepared using different polymers were tested for in vitro release of ibuprofen in triplicates in phosphate buffered saline (PBS, 10 mM, pH 7.4.). We suspended 150 mg of NPs in 3.5 mL PBS in a dialysis tubing (Spectra Por 1 membrane, 6–8 kDa cut-off). This dialysis tubing was placed in a screw-capped tube containing 10 mL PBS. The tubes were shaken at200 rpm on a horizontal water bath shaker (Orbit Shaker Bath, Labline) maintained at 37 ± 0.5 °C. At predetermined time intervals, the whole medium in the tube was withdrawn and replaced by fresh PBS to maintain sink conditions. The aliquots were assayed for the concentration of ibuprofen released by spectrophotometry at 262 nm.

3. Results and discussion

3.1. Characterization of polymers

^{1}H NMR spectroscopy and gel permeation chromatography (GPC) were used to measure the number average (M_n) and weight average molecular weights (M_w) of the synthesized polymers. The polydispersity was calculated by the ratio of M_w to M_n from the GPC data. All the synthesized polymers exhibited uniform molecular weight distribution as revealed by the narrow polydispersity index values (Table 1). Unimodal mass distribution ruled out the possibility of the presence of unreacted MePEG or Poly(D, L-lactide) in case of PEG7%-g-PLA. The results are summarized in Table 1. Typical ^{1}H NMR spectrum was obtained for PLA homopolymer with a characteristic peak at 5.2 ppm corresponding to the tertiary PLA proton (m, –CH), and another peak at 1.5 ppm for the pendant methyl group of the PLA chain (m, $–CH_3$). Moreover, the integration ratio of those two characteristic peaks was 3:1 that is also a characteristic feature for the protons of PLA homopolymer (data not shown). ^{1}H NMR spectra and chemical structures of PEG7%-*g*-PLA and (PLA–PEG–PLA)*n* polymers are shown in Fig. 1. Also typical spectrum for PEG7%-g-PLA was obtained with a peak at 5.2 ppm corresponding to the tertiary PLA proton (m, –CH), a peak at 3.6 ppm for the protons of the repeating units in the PEG chain (m, $OCH_2–CH_2O$), a peak at 4.3 ppm for the PEG connecting unit to the PLA block (m, $CH_2–OCO$), and a peak at 1.5 ppm for the pendant methyl group of the PLA chain (m, $–CH_3$). While, for the multiblock copolymer, an additional peak could be seen at around 2.7 ppm corresponding to the protons of the succinic acid group (m, $CH_2–COO$) used to link the triblock chains during multiblock synthesis. The actual PEG insertion ratio of PEG7%-g-PLA and (PLA–PEG–PLA)*n* was calculated by comparing the peak intensity

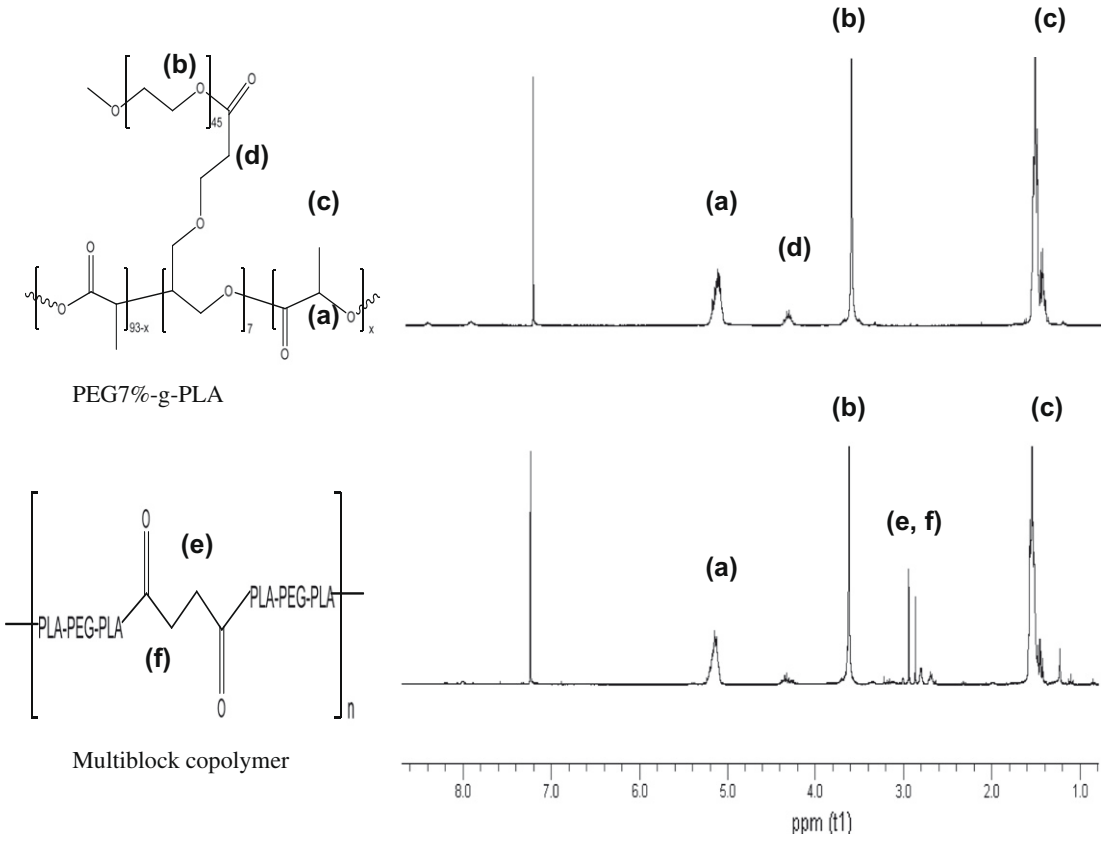

Fig. 1. ^{1}H NMR spectra and chemical structures of PEG7%-g-PLA, and multiblock copolymer (PLA–PEG–PLA)*n*.

ratios of PEG (3.6 ppm) to that of PLA (5.2 ppm). The final PEG insertion ratio in both polymers was close to the initial feed ratio as shown in Table 1.

3.2. Particle size and size distribution

Particle size distribution by dynamic light scattering (DLS) showed unimodal distribution for freshly prepared as well as lyophilized NPs. Freshly prepared (PLA–PEG–PLA)*n* NPs either blank or loaded showed larger hydrodynamic diameter (~200 nm) than PEG7%-*g*-PLA NPs (~135 nm) as shown in Table 2. The last finding could be attributed to the difference in PEG chain organization during NPs formation between both formulations. In PEG7%-g-PLA, PEG chains are expected to be more mobile, creating a steric barrier around PLA core preventing particle aggregation. While, for multiblock copolymer, the polymer architecture allows some PEG chains to be embedded inside PLA core leaving some uncovered areas at the surface that might showed some aggregating tendency due to hydrophobic interactions. Moreover, the higher PEG content of multiblock copolymer (8.9%, Table 1) might favor the swelling of NPs in aqueous media to a much degree than PEG7%-g-PLA NPs which contains lower PEG ratio (4.1%, Table 1). Blank formulations showed nearly similar particle size to that of loaded ones for all NPs types in the range of 135–200 nm (Table 2). Thus, drug loading level had no apparent effect on particle size, suggesting that the size was largely controlled by the emulsification process during NPs preparation. Also, it could be noticed that the size of most lyophilized NPs after resuspension into Milli-Q Water was smaller with narrow polydispersity compared to the freshly prepared NPs suspension. The possible reason behind that is the tendency of freshly prepared

Table 2
Characteristics of different NPs formulation.

Formulation	Size before freeze-drying (nm)[a,d]	PI [b]	Size after freeze-drying (nm)[a,d]	PI[b]	Actual loading (% wt/wt)[d]	% EE[c,d]	Zeta potential (mV)[a,d]	Surface-associated PVA (% wt/wt)[d]
PLA BK[e]	184 ± 20.8	0.13	161 ± 18.4	0.01	N/A	N/A	−3.5 ± 3.1	6.76 ± 0.40
PLA LD[f]	194 ± 30.0	0.08	162 ± 22.3	0.09	4.5 ± 0.22	45 ± 2.24	−0.18 ± 3.2	6.80 ± 0.20
PEG7%-g-PLA BK[e]	132 ± 28.0	0.16	166 ± 30.5	0.01	N/A	N/A	−2.2 ± 3.0	3.57 ± 0.60
PEG7%-g-PLA LD[f]	145 ± 34.0	0.07	137 ± 82.1	0.04	7.9 ± 0.04	79.7 ± 0.56	−0.2 ± 3.1	3.79 ± 0.50
(PLA–PEG–PLA)*n* BK[e]	202 ± 21.2	0.01	168 ± 42.1	0.01	N/A	N/A	−1.0 ± 3.5	0.40 ± 0.50
(PLA–PEG–PLA)*n* LD[f]	199 ± 19.8	0.10	158 ± 31.9	0.02	2.5 ± 0.12	25.3 ± 1.20	−0.24 ± 3.2	0.70 ± 0.60

N/A: Not analyzed.
NB: (PLA–PEG–PLA)*n* consists of 1:1 mixture of PLA: (PLA–PEG–PLA)*n*.
[a] Median.
[b] Refers to polydispersity index.
[c] Refers to encapsulation efficiency.
[d] All values indicate mean ± SD for $n = 3$ independent measurements for the same particle preparation.
[e] Blank NPS.
[f] Loaded NPS.

PLA particles particularly pegylated ones to uptake water, allowing more swelling of the NPs matrix [11,12], further increasing the size of the particles. While, after lyophilization, the size of the particles was reduced due to shrinkage of the swollen cores after removal of entrapped water by sublimation. The narrow polydispersity values indicate the ability of the used cryoprotectant used (sucrose) to prevent particle aggregation. It was previously reported that cryoprotectants could efficiently prevent NPs aggregation and protect them against the mechanical stress of ice crystals due to the immobilization of nanoparticles within their glassy matrices [13]. Particle size distribution data by DLS were also supplemented with a visual method like tapping mode AFM as will be revealed in the next section.

3.3. Surface morphology and phase analysis

Tapping mode atomic force microscopy (TM-AFM) is a versatile technique, which allows probing soft samples such as biological and polymeric materials [14,15]. TM-AFM surface analysis revealed that all lyophilized NPs were nearly spherical with smooth surface and displayed less aggregating tendency with a size range 100–200 nm (Fig. 2, left panels, T) confirming the size data obtained by DLS. Phase image analysis using the same (TM-AFM) was done on NP samples to visually examine PEG chains at the surface of pegylated NPs. Phase imaging is based on the use of changes in the phase angle of cantilever probe. This image shows more contrast than the topographic one as well as more sensitivity to material surface properties such as stiffness, viscoelasticity, and chemical composition [14,16,17]. Fig. 2 shows TM-AFM topography (left panel, T) and their corresponding phase images (right panel, P) of PLA, PEG7%-*g*-PLA, and multiblock copolymer, respectively, acquired at moderate tapping force. It can be seen that PLA particles had nearly homogenous surface without any clear phase separation [Fig. 2a; right panel, P). Therefore, no contrast was observed in phase images of PLA NPs. On the other hand, both pegylated NPs showed the presence of an observable phase contrast at the surface of NPs that varies in degree from grafted to multiblock [Fig. 2b and c; right panels, P]. This might be due mechanical differences between PLA and PEG that result in such phase contrast. PEG molecule is expected to be softer than PLA since PEG molecules of lower M_w 2000 or 1500 (used in our study) have smaller Young's modulus than PLA [18]. Thus, it was expected that PEG molecule will appear as darker regions in the phase images due to negative phase shift. This has already been shown before for poly(styrene-b-ethylene oxide) polymer films, where softer PEG segments appeared as darker regions embedded in lighter polystyrene domain [19]. In the case of PEG7%-g-PLA, highly intense dark coat surrounds the surface of brighter core could be seen indicating the existence of hydrophilic PEG chains around hydrophobic PLA chains that represents the core. The immiscibility of these two blocks should result in separation of both components during NPs formation. Thus, grafted copolymer NPs will be predominantly consisting of hydrophobic PLA cores surrounded by hydrophilic PEG chains on the surface (Fig. 2b, phase image, P). In the case of the (PLA–PEG–PLA)*n* multiblock copolymer, few dark regions are found at the surface of NPs without complete coverage of the surface as seen with grafted polymer. This might be due to the peculiar architecture of the polymer itself that mainly consist of PEG chain covalently linked with two PLA chains. This might affect mobility of PEG chains towards the aqueous phase of the O/W emulsion during NPs formation. It was shown before in a previous study that multiblock copolymers of PLA and PEG exhibited enhanced miscibility of the two blocks compared to grafted copolymers [20].

3.4. Encapsulation efficiency (EE)

As seen from Table 2, %EE of ibuprofen was found to be 25.3% and 79.7% for multiblock and PEG7%-*g*-PLA NPs, respectively. PEG7%-*g*-PLA showed better %EE than multiblock copolymers. The last finding could be attributed to the enhanced steric hindrance of the more mobile PEG chains at NPs surface in the case of the grafted copolymers, thus reducing premature diffusion of ibuprofen into the external aqueous phase during solidification of the NPs. This was confirmed before by AFM phase imaging where PEG chains were found to completely cover the entire NPs surface. The higher encapsulation efficiency obtained with PEG7%-g-PLA may have significant implications on the feasibility of development of PLA–PEG nanoparticulate formulations optimized with regard to

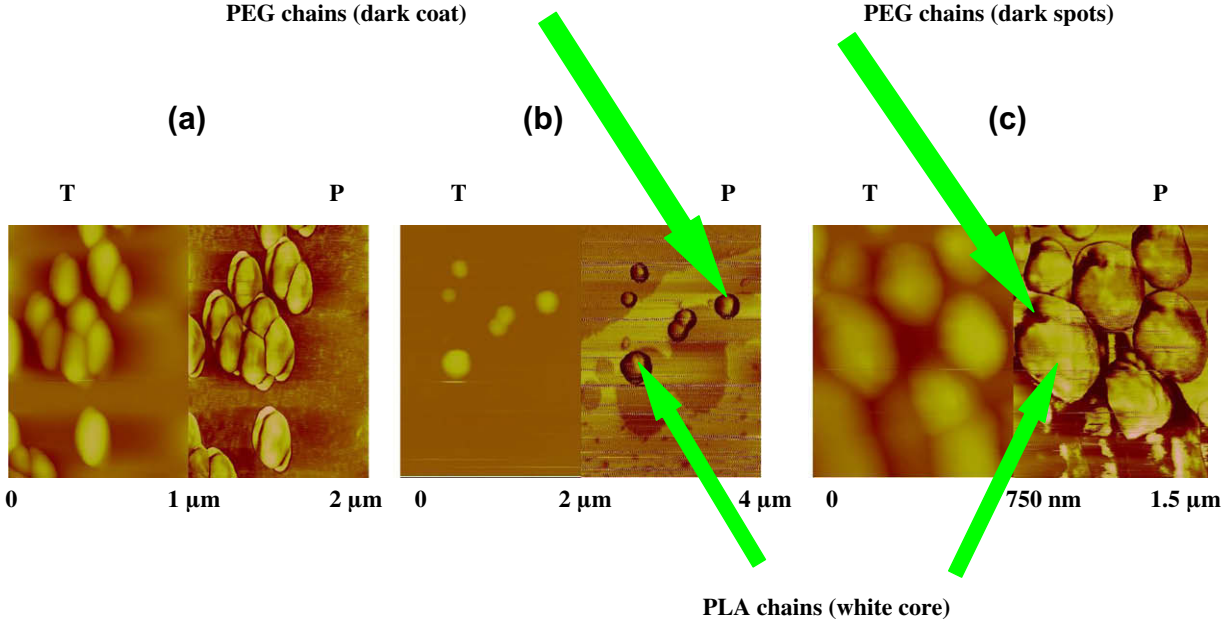

Fig. 2. Tapping mode AFM images of NPs, left panel shows topography (T) and right panel shows corresponding phase images (P); all images are acquired in air. PLA (a) [Scan size: 1 µm × 1 µm], PEG7%-g-PLA, (b) [scan size: 2 µm × 2 µm], and (PLA–PEG–PLA)*n*, and (c) [scan size: 750 nm × 750 nm]. (For interpretation of the references to color in this figure legend, the reader is referred to the web version of this article.)

both the longer circulation behavior and the drug loading properties by judicious selection of both the composition and the suitable architecture of the nanoparticles. Thus, the obtained data suggest that it is possible to prepare nanoparticles with low PEG content, which would generate favorable conditions for the entrapment of a hydrophobic drug, without compromising the prolonged blood circulation properties of the nanoparticles.

3.5. Zeta (ζ) potential measurements

Although zeta potential measurements did not show big differences between different formulations but two findings worthy of note were observed in Table 2: (1) PLA showed low zeta potential (close to zero) values than expected, −3.5 mV. This lower ζ-potential for NPs could be attributed to the effective adsorption of PVA on the surface of NPs as will be seen in the next section which could mask the surface charge of PLA. Zambaux et al. also obtained a low zeta potential value of −4 mV for PLA NPs prepared with PVA as an emulsifier [21]. (2) Pegylated polymers either grafted or block had also low zeta potential values for both blank and loaded NPs as shown in Table 2. This could be attributed to the shielding action of PEG on the surface charge even if most of PEG chains were found embedded into the NPs matrix as in case of multiblock copolymer. Since some of the PEG chains would be present at the surface, the copolymer might also keep its stealth behavior. Similar results to ours were reported earlier by other authors [9,22,23]. Moreover, the greater reduction in zeta potential values of pegylated NPs compared to other PEG–PLA NPs reported in the last cited references could be explained by the existence of a fraction of PVA at the surface of NPs which played also a role in masking their actual surface charge (Table 2). It also should be mentioned that zeta potential measurements were done again in 0.5 mM NaCl solution in order to clearly find significant differences between different NPs formulations. However, nearly similar zeta potential values to the ones observed with 0.25% w/v NaCl were obtained (data not shown).

3.6. Residual PVA

It is widely reported that although the several washing steps of nanoparticles, yet some residual surfactant remains in the suspension and becomes adsorbed onto surface of freeze dried nanoparticles and this might lead to alteration of their physicochemical properties such as particle size, hydrophilicity, release kinetics, and cellular uptake [7]. So, one of our goals was to evaluate the amount of PVA remained attached to the nanoparticles and whether they are affected by different PEG chain organization of the polymer or not. It was observed that a variable amount of PVA remained in all the formulations even after four washings (Table 2). An attempt was made to evaluate whether PVA was present either inside the polymeric matrix or on the surface of the particles. Nearly the same amount of PVA was present in the given NPs formulations by both assays confirming that the amount of PVA was mainly associated with the surface of the particles (data not shown). It was found that the highest amount of PVA remained attached to NPs matrix was 6.7% wt/wt for PLANPs (Table 2). This might be attributed to the enhanced hydrophobic interaction between acetate group of PVA and the hydrophobic PLA matrix as reported before by other authors [7,24]. This result is in accordance with other previous studies by other authors. Sahoo et al. [7] have determined 6.15% wt/wt PVA remaining associated within PLGA NPs matrix when they used 5% PVA solution as external aqueous phase. Another study done by Zambaux et al. showed also that 5–6% wt/wt PVA remained attached within PLA NPs after three washings when 1% PVA was used as an external aqueous phase [21]. For all the other pegylated polymers either graft or block, they exhibited less adsorption of PVA than PLA NPs as shown in Table 2. This might be due to the PEG content which offered a certain degree of hydrophilicity to the NPs matrix so a less favored interaction with PVA should be expected. Similar results were obtained before where the amount of adsorbed PVA decreased with increased PEG content within the NPs matrix [10]. Multiblock copolymer NPs showed less PVA adsorption ∼0.5% compared to PEG7%-g-PLA which showed ∼3.5% wt/wt. The reason behind that is the possibility of a chemical interaction between PVA-OH and PLA-COOH, and this interaction might be less favored in case of multiblock copolymer NPs as will be revealed by XPS data. Also, blank NPs showed similar amount of PVA adsorbed on their surfaces as loaded NPs indicating that drug loading had no apparent effect on the amount or the orientation of PVA within the NPs matrix.

3.7. DSC

DSC was used to detect the effect of molecular structure of the used polymer on the thermal properties of NPs. Moreover, DSC was also used for detecting the state of the encapsulated drug inside the NPs matrix as well as investigating any possible interaction between the drug and the polymeric matrix. PLA showed glass transition (T_g) at 46.4 °C (Table 1). Grafting PEG on the PLA backbone resulted in an increased T_g value (by about 7 °C) due to enhanced chain rigidity (Table 1 and Fig. 3a). Similar findings were previously reported for hyperbranched polymers and dendrimers over their linear chain analogues [25]. However, multiblock copolymer showed lower T_g values at 39 °C, compared to grafted polymer (Table 1 and Fig. 3b). This might be attributed to their actual higher PEG content 8.9 mol% and/or low molecular weight when compared to the grafted polymers (Table 1). Also, this might indicate the presence of some PEG chains inside the core of PLA. The high PEG content embedded inside PLA chains might enhance the chain mobility of PLA due to its plasticization effect on PLA chains resulting in a lower T_g, as reported earlier [26,27]. Thus, the effect of branching was predominant for PEG grafting over PLA backbone, whereas the possibility of PEG chains entrapment inside PLA domains might lead to a predominant plasticizer effect. Ibuprofen showed an endothermic peak at 78 °C corresponding to the melting of ibuprofen crystals (Fig. 3a and b). As shown in Fig. 3a, DSC curve of PEG7%-g-PLA/ibuprofen physical mixture showed an endothermic peak corresponding to the glass transition (T_g) at ∼52 °C. The melting endotherm of ibuprofen crystals could also be detected at 74 °C. The drug melting peak was shifted by 4 °C lower with some broadening of the peak, indicating the possibility of a weak interaction between the drug and the polymer. After encapsulation of ibuprofen into the NPs, T_g was found to be ∼20 °C, which might be due to process formulation parameters. Surprisingly, the melting endotherm of the drug was clearly observed with also some broadening of its melting peak (Fig. 3a). This phenomenon has been related recently to the size of the nanocrystals obtained after the process of encapsulation [28]. For more verification of the final state of ibuprofen inside NPs, X-ray diffraction analysis (XRD) was carried out for ibuprofen-loaded NPs and compared to both pure ibuprofen crystals and physical mixture of the polymer with the drug having the same ratio as in NPs. Ibuprofen-loaded NPs showed the presence of crystalline ibuprofen but with slight reduction in the intensity of its diffraction peaks (Figure S in the supporting information). XRD data confirmed DSC findings. Similar observations were also noticed with (PLA–PEG–PLA)*n*, in both physical mixtures and NPs with the consideration of different T_g for multiblock copolymer ∼39 °C (Fig. 3b). Similar finding to ours was obtained when lidocaine embedded into PEG–PLGA nanospheres. Lidocaine exhibited an endothermic peak at lower temperature or broadened melting peak compared to lidocaine alone.

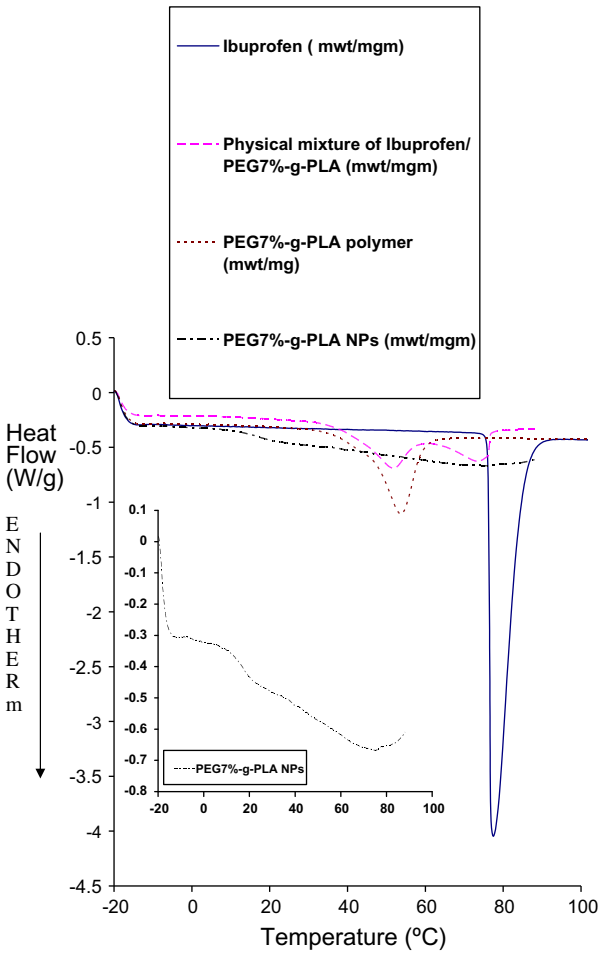

Fig. 3a. DSC curves of ibuprofen, physical mixture of PEG7%-g-PLA with ibuprofen, PEG7%-g-PLA polymer, and ibuprofen-loaded NPs. Inset inside the figure shows clear thermogram for NPs. (For interpretation of the references to color in this figure legend, the reader is referred to the web version of this article.)

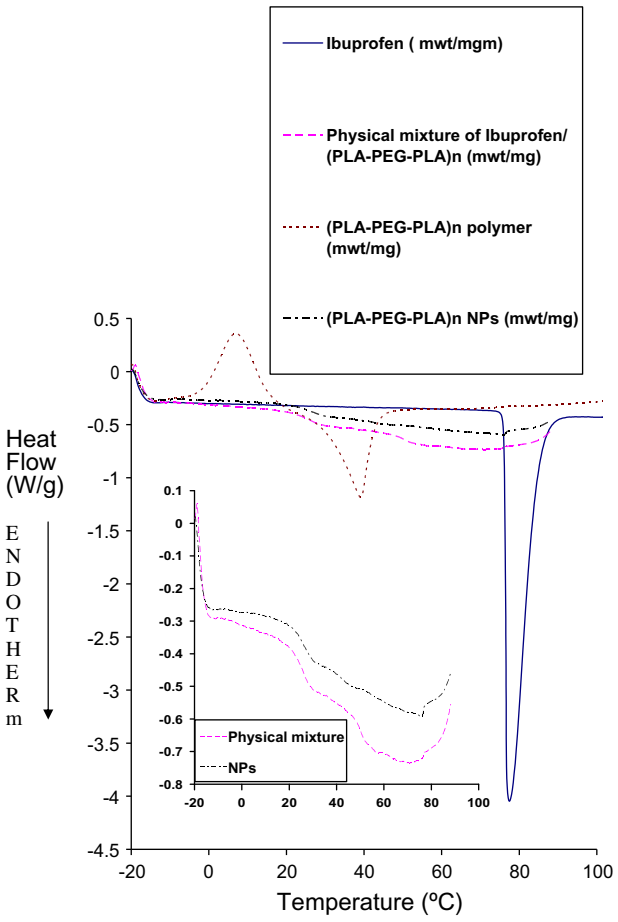

Fig. 3b. DSC curves of ibuprofen, physical mixture of (PLA–PEG–PLA)*n* with ibuprofen, (PLA–PEG–PLA)*n* polymer, and ibuprofen-loaded NPs. Inset inside the figure shows clear thermograms for both physical mixtures and NPs. (For interpretation of the references to color in this figure legend, the reader is referred to the web version of this article.)

The authors also suggested that there is an interaction between lidocaine and the polymeric carrier [2].

3.8. XPS analysis

XPS analysis was done to investigate the surface chemistry of NPs prepared from different polymers and to detect any possible interaction between PLA and PVA on their surface. XPS spectrum of PEG showed one characteristic peak corresponding to ether carbons (286.5 eV, Table 3). PVA polymer showed three main characteristic peaks corresponding to C–C/C–H (285 eV), C–OH (286.7 eV) and O–CO (289 eV) components (Table 3). For synthesized PLA homopolymer, the best envelop fit was obtained using three main peaks corresponding to C–C/C–H (285 eV), C–OH (287 eV) and O–C═O (289 eV) (Table 3). Similar results were obtained before with Shakesheff et al. [10]. Ibuprofen could not be experimentally analyzed since it was found to sublime under the high vacuum of the equipment. Based on theoretical estimation, ibuprofen has two main characteristic peaks corresponding to C–C/C–H (285 eV), and O–C═O (289 eV) components (Table 3). It should be mentioned that for ibuprofen to be detected at the surface of loaded NPs, an increase in atomic percentages of both its characteristic peaks mainly C–C/C–H (285 eV) is expected to be found. Both ibuprofen-loaded and blank NPs of **PEG7%-g-PLA**-grafted polymer as well as the polymer itself showed the existence of PEG chains on the surface as seen by the presence of a characteristic peak corresponding to ether carbons (286.5 eV, Table 4). However, the atomic% of PEG decreases from the polymer (16.9%) to blank (11.8%) then to loaded NPs (8%) as shown in Table 4. This might be due to adsorption of PVA in case of blank NPs. While in loaded NPs, both PVA and ibuprofen might be adsorbed at the surface of NPs as evidenced from the increase in atomic% of C–C (285 eV) in case of loaded NPs (18.6%) compared to blank NPs (13.1%) [Table 4]. Such an adsorption might decrease the PEG content at the surface. Also, it could be seen from Table 4 that the atomic% of C–C (285 eV) decreases from the polymer (18%) to blank (13.1%) and then increased again in case of loaded NPs (18.6%). This order might be due to chain organization during NPs formation by O/W emulsion method in such a way that PLA chains (rich in C–C) will be collapsed inside the oil droplets (internal phase) while PEG chains will be facing the external aqueous phase. Oil droplets tend to form the internal NPs core upon organic solvent removal and particle precipitation. This process will lower PLA chains and hence, C–C content at the NPs surface. This C–C content lowering was compensated by drug adsorption (also rich in C–C component as shown in Table 3) at the surface in case of loaded NPs as stated before. Moreover, to get the best envelop fit of both NPs, two additional peaks had to be added corresponding to C–O–*C═O (287.6 eV) and *C–O–C═O (286.2 eV) components (Table 4). These new peaks obtained in both types of NPs could be the result of chemical interaction between PLA-COOH end and PVA-OH during NP formation. The last finding also supports the

Table 3
Relative atomic percentages calculated from XPS surface analysis of pure materials used in NPs formulation.

Binding energy (functional component)	Atomic percentage (%)			
	Ibuprofen	PLA	PVA	PEG
285 (C–C)	92.4	22.3	37.1	–
286.5 (C–O)	–	–	–	100
286.7 (C–O)	–	–	23	–
287 (C–O)	–	28.9	–	–
289 (O–C=O)	7.6	13.9	4.3	–

NB: Relative percentage of each functional component is calculated from the area under the curve from their respective peaks in XPS analysis.

effective masking of negative charge of these NPs by both PEG and PVA chains at the surface of such NPs as shown in Table 2. The increase in atomic% of O–C=O (289 eV) from the polymer (5%) to both blank and loaded NPs (7.1% and 6.9%, respectively) might be due to PVA (partially hydrolyzed) and ibuprofen (weak acid) adsorption at the surface of blank and loaded NPs types, respectively. This O–C=O (289 eV) component was also detected in the XPS spectrum of the polymer itself due to the presence of COOH functional group in the polymer structure (Fig. 1). On the other hand, both drug-loaded and blank NPs of **(PLA–PEG–PLA)*n*** polymer as well as the polymer itself showed also the existence of PEG chains on the surface as evidenced from the presence of the same characteristic peak corresponding to ether carbons of PEG (286.5 eV, Table 4). However, the atomic% of PEG was markedly decreased upon NPs formation compared to grafted polymer. PEG atomic% detected in the polymer was (31.2%) compared to blank (13%) and loaded NPs (11.6%). Taking into account that minimal amount of PVA was detected at the surface of multiblock NPs (~0.5% wt/wt, Table 2), so the last finding indicates that only a small fraction of the total PEG content of the multiblock copolymer exists at the surface of NPs while the remaining PEG chains might be entrapped inside NPs core. This could be also due to chain organization during NPs formation by O/W emulsion method in such a way that showed the difficulty of PEG chains migration towards the surface of NPs. In fact, the peculiar architecture of the multiblock copolymer (PLA–PEG–PLA)*n* shows that PEG chains are covalently linked between two neighboring PLA chains. That is why PEG chains are not easy to orientate towards the surface of NPs facing the aqueous phase and most of them is orientated or stretched more towards the core. AFM phase images of multiblock copolymer showed the existence of few PEG chains at the surface of NPs compared to grafted polymer confirming XPS findings (Fig. 2). Moreover, no additional peaks were needed to complete the fit indicating the absence of PLA interaction with PVA in multiblock copolymer NPs. This might be due to the lower number of free COOH end components available for reaction with PVA-OH components in multiblock copolymer NPs in contrast to grafted polymers. Since multiblock copolymer has been synthesized by the condensation of triblock copolymer, the number of available COOH components was expected to be low. The last hypothesis was supported by the lower atomic% of O–C=O (289 eV) component at the surface of the polymer (2.1%), blank (2.3%), and loaded NPs (3.2%), respectively. The atomic% of C–C (285 eV) was detected in the XPS spectrum of blank NPs in a similar value to that of the polymer (19%) due to presence of some PLA chains (rich in C–C) at the NPs surface since PEG does not cover the NPs surface completely. While, the increase in atomic% of C–C components (285 eV) in case of loaded NPs (21.8%) confirms the possibility of drug existence at the surface of NPs.

3.9. ^1H NMR of NPs in D_2O

^1H NMR analysis was done on NPs in attempt to investigate the core–corona structure of pegylated NPs. ^1H NMR spectra of all pegylated NPs in D_2O showed presence of methylene protons of PEG chains at 3.6 ppm (Fig. 4). Signals from PLA methyl or methylene protons were absent or diminished in intensity. This might indicate that PLA protons are in solid environment and cannot be detected whereas PEG chains must be in mobile state. ^1H NMR analysis for PLA–PEG diblock NPs confirmed their core–corona structure [29]. Similar finding was obtained for NPs made from comb polyesters of PVA-g-PLGA in water showing reduced signal intensity of the more hydrophobic PLGA chains compared to hydroxyl terminated end groups of PVA [30]. Our results are in

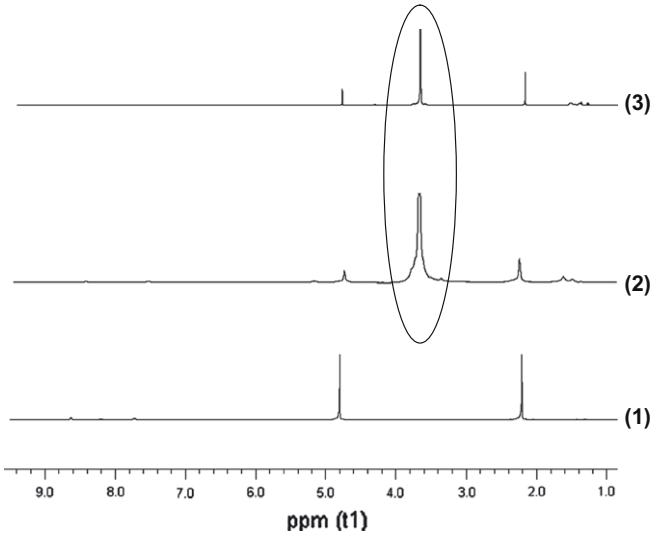

Fig. 4. ^1H NMR of blank NPs of PLA (1), PEG7%-g-PLA (2), and (PLA–PEG–PLA)*n* (3) in D2O. PEG peaks at 3.6 ppm are encircled.

Table 4
Relative atomic percentages calculated from XPS surface analysis of synthesized polymers and formulated NPs using those polymers.

B.E. (functional component)	Atomic percentage (%)					
	PEG7%-g-PLA BK NPs	PEG7%-g-PLA LD NPs	PEG7%-g-PLA polymer	(PLA–PEG–PLA)*n* BK NPs	(PLA–PEG–PLA)*n* LD NPs	(PLA–PEG–PLA)*n* polymer
285 (C–C)	13.1	18.6	18	19	21.8	19.2
286.2 (*C–O–C=O)	10.1	10.4	–	–	–	–
286.5 (C–O)	11.8	8	16.9	13	11.6	31.2
287.6 (C–O–*C=O)	7.1	6.9	–	–	–	–
289 (O–C=O)	7.1	6.9	5	2.3	3.2	2.1

(BE) refers to the binding energy.
(BK) refers to blank NPs.
(LD) refers to loaded NPs.

accordance with the above-cited reference suggesting NPs made of PLA core and PEG corona. Thus, ^{1}H NMR analysis of NPs might indicate that hydrophilic polymer parts (PEG) are oriented towards the outer phase (water) during precipitation and NP hardening whereas the more lipophilic polyester PLA residues form the inner core. However, these studies are not quantitative to comment whereas all the PEG chains constitute the corona and to determine the amount of PEG exactly at the surface for both grafted and block pegylated NPs.

3.10. Erosion study

This study was conducted to investigate the effect of PEG chain organization on the degradation rate of PLA-based NPs under conditions similar to physiological ones. Mass loss of copolymer in phosphate buffer started after 5 days for all the investigated NPs. Pegylated NPs showed faster degradation rates (30% and 44% for PEG7%-g-PLA and (PLA–PEG–PLA)*n*, respectively) compared to PLA NPs which showed slower degradation rates around 12% after 25 days. This pattern is shown in Fig. 5. Ester hydrolysis and transesterification mechanisms are both responsible for mass loss of polyester copolymers [31]. NPs erosion was initiated by water uptake followed by random hydrolytic chain scission of PLA block with release of lactide oligomers. So, it might be expected that the more hydrophilic polymer initially swells to a much greater degree than other polymers of lower hydrophilic content, allowing more water uptake into the matrix, further increasing the rate of hydrolysis and breakdown of NPs [11,32]. Cleavage of the ester bonds between the PLA–PEG backbone leads to free PEG units that will be formed and diffuse out of the matrix. With the loss of PEG from the backbone, degradation of the matrix is dominated by PLA with an increase of the internal matrix-surface in contact with water leading to higher degradation rates than that of homopolymer [33]. The faster degradation rate of (PLA–PEG–PLA)*n* NPs (44%) compared to PEG7%-g-PLA(30%) after 25 days emphasizes the rapid core (PLA) wetting in the multiblock copolymer NPs. This might be due to entrapment of most of PEG chains into the NPs core while in case of grafted PEG7%-g-PLA polymer, most of PEG was found to be at the surface of NPs as shown before by AFM phase imaging and XPS studies.

3.11. In vitro drug release

In order to study the effect of PEG chain organization on drug release profiles from different PLA NPs, ibuprofen-loaded NPs were compared for their in vitro release behavior as shown in Fig. 6. It could be seen that all formulations exhibited biphasic release phenomenon. After 8 h of NPs immersion into the release medium, a rapid initial burst of ibuprofen varied from 20% to 53% of the drug content was clearly observed in all batches. This finding might be due to the desorption of the drug particles adsorbed at or close to the surface of NPs[34] followed by sustained release of the drug over 300 h. This second sustained release phase would mainly depend on both drug diffusion and the matrix erosion that was a slower process [35,36]. In such case, the effects of porosity of the nanoparticles on the release property should be verified. As mentioned earlier in experimental section, we used 5% w/v sucrose as cryoprotectant to prevent NPs aggregation during lyophilization. Such higher concentration was found to have pore blocking action particularly surface pores, an effect caused by the precipitation of cryoprotectant on nanoparticle surface [37]. So, we expected that NPs porosity might have a minor effect on ibuprofen release from NPs. Thus, the last hypothesis might support that the slow release of drug might be mainly controlled by both solubility of the drug in the matrix and matrix erosion mechanism. The physical state of the drug inside the NPs matrix was investigated before using DSC since this would have an influence on the in vitro and in vivo release characteristics of the drug. DSC indicated that ibuprofen exists in a crystalline state inside all NPs irrespective of their polymer content. The last finding indicates that the main rate limiting step affecting drug release will be the dissolution of drug crystals into the polymeric matrix followed by their diffusion out of the matrix into the release media. This finding also confirmed the role of NPs core wetting in enhancing drug dissolution and hence drug release. Thus, the polymer that favors more water uptake and hence rapid core wetting would facilitate drug dissolution and hence faster drug release. The release pattern for all NPs formulations showed good correlation coefficient (R^2 was close to 1) when fitted to Higushi square root equation of diffusion (data not shown) indicating that release will be mainly dominated by the diffusion of the solubilized drug crystals through the NPs matrix with some contribution from degradation decreasing in

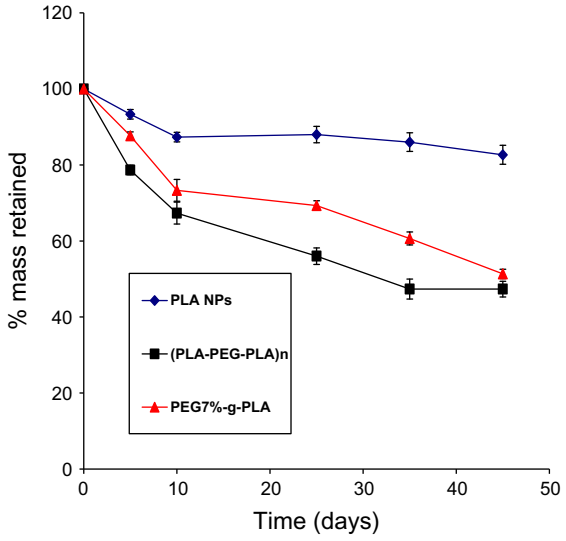

Fig. 5. Erosion of different ibuprofen-loaded NPs in phosphate buffer saline (PBS, pH 7.4) at 37 °C. (For interpretation of the references to color in this figure legend, the reader is referred to the web version of this article.)

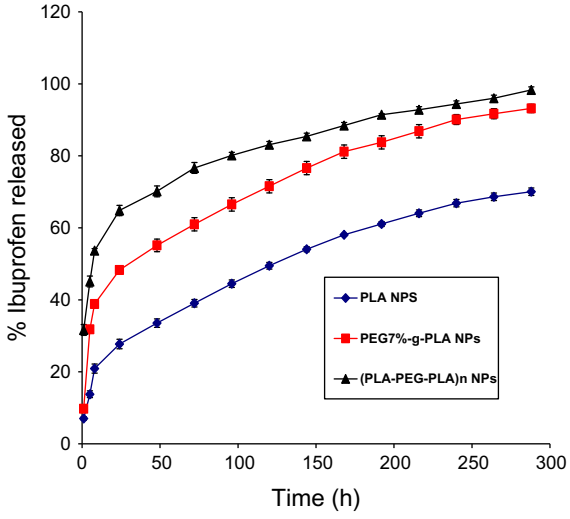

Fig. 6. Effect of PEG chain organization on the in vitro release behavior of ibuprofen-loaded NPs; values are represented as mean ± SD of three independent experiments. (For interpretation of the references to color in this figure legend, the reader is referred to the web version of this article.)

importance upon increasing the molecular weight of the polymer [36]. It could be seen that multiblock copolymers NPs showed faster drug release compared to PEG7%-g-PLA NPs. The possible reason behind that is the peculiar polymer architecture of the multiblock copolymer allows a major portion of PEG to be entrapped inside the core during NP formation as revealed from XPS and phase imaging data and hence, rapid wetting of the core will take place compared to grafted NPs. When PEG7%-g-PLA NPs are suspended into the release medium, a major fraction of PEG will be migrated easily towards the surface while the cores will be predominantly hydrophobic. In case of multiblock, a considerable amount of PEG is expected to be embedded into the PLA core due to the covalent linkage of PEG with two PLA blocks as stated before which might hinder PEG chains to be migrated towards the surface. The hydrophilicity of the matrix is one of the major factors that markedly influence its hydration and, in turn, the drug release profile [38,39]. Multiblock copolymer NPs were shown in the last section to erode faster than PEG7%-*g*-PLA NPs confirming the faster release rate obtained with such NPs. Another previous study showed that multiblock copolymers of PEG and PLA exhibited faster drug release compared to their PLA homopolymer and the authors attributed this also to the marked hydrophilic properties of multiblock copolymers [40,41]. These results showed that core wetting is an important factor influencing the drug release kinetics. A schematic representation of different NPs chain organization depending on both their polymer composition and architecture is shown in Fig. 7. This difference in chain organization was found to have an effect on the release kinetics of the encapsulated drug from NPs. Generally speaking, our results suggest the possibility of use of such pegylated NPs as drug carrier for poorly soluble drugs. Also, they could have the potential of targeting the encapsulated drugs into certain tissues depending on their ability to circulate for longer periods of time without being recognized by the immune system. It should also be mentioned that the use of multiblock copolymer would facilitate the encapsulation of hydrophilic drugs into their NPs matrix due to the formation of small pockets of PEG that might create an aqueous phase embedded inside a hydrophobic polymeric matrix.

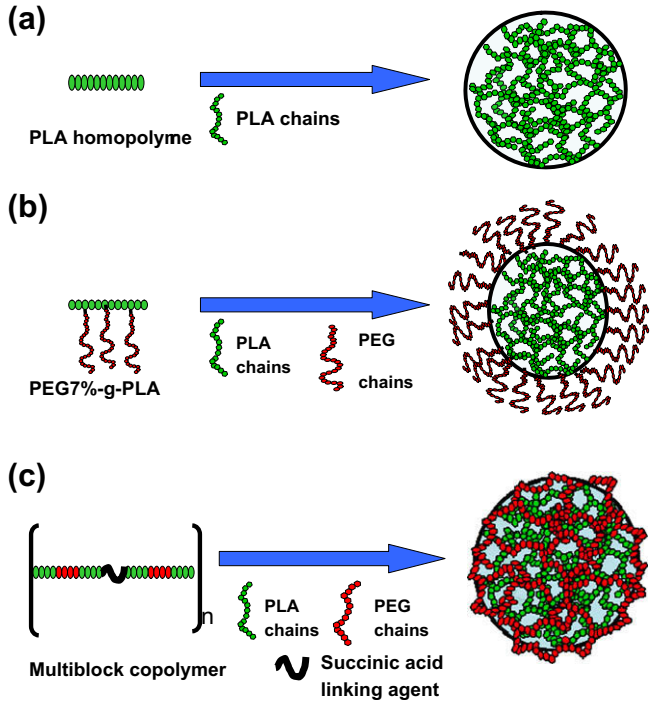

Fig. 7. Schematic representation of polymer chain organization inside the NPs: PLA (a), PEG7%-g-PLA (b), and multiblock copolymers (PLA–PEG–PLA)*n* (c). (For interpretation of the references to color in this figure legend, the reader is referred to the web version of this article.)

4. Conclusion

NPs were fabricated using novel copolymers of PEG-modified PLA polymers with different PEG chain organization. Both AFM phase imaging and XPS studies showed the existence of PEG chains on the surface of grafted pegylated NPs. Both studies also showed that multiblock copolymer displayed less amount of PEG on the surface due to the possibility of PEG chains interpenetration inside the PLA core of NPs. This resulted in lower T_g, rapid degradation of the polymeric matrix, and faster drug release from NPs. On the contrary, grafted pegylated copolymer showed enhanced immiscibility of both PEG and PLA blocks resulting in enhanced phase separation of both components during NPs formation and hence, easy migration of PEG chains towards the surface of NPs while the cores will be predominantly hydrophobic. Our future work will focus on studying the cellular uptake of rhodamine encapsulated NPs made from different polymers with different PEG chain organization. In brief, the way PEG chain organized onto PLA backbone is an important parameter controlling surface characteristics of NPs which in turn determine their physicochemical properties like encapsulation efficiency, % PVA adsorbed at the surface of NPs, zeta potential, thermal characteristic, and drug release kinetics.

Acknowledgments

This work was supported in part by a grant of Fond Quebecois de la Recherche en Nature et Technologie (FQRNT). The authors wish to thank Mme. Suzie poulin, research associate at École Polytechnique, University of Montreal for her help in the data analysis of the XPS experiments. Sherief Essa thanks the Ministry of Higher Education, Egypt for granting him a scholarship during his Ph.D.

Appendix A. Supplementary material

Supplementary data associated with this article can be found, in the online version, at doi:10.1016/j.ejpb.2010.03.002.

References

[1] S.R. Popielarski, S.H. Pun, M.E. Davis, A nanoparticle-based model delivery system to guide the rational design of gene delivery to the liver. 1. Synthesis and characterization, Bioconjugate Chemistry 16 (2005) 1063–1070.
[2] M.T. Peracchia, R. Gref, Y. Minamitake, A. Domb, N. Lotan, R. Langer, PEG-coated nanospheres from amphiphilic diblock and multiblock copolymers: investigation of their drug encapsulation and release characteristics, Journal of Controlled Release 46 (1997) 223–231.
[3] Y.-P. Li, Y.-Y. Pei, X.-Y. Zhang, Z.-H. Gu, Z.-H. Zhou, W.-F. Yuan, J.-J. Zhou, J.-H. Zhu, X.-J. Gao, PEGylated PLGA nanoparticles as protein carriers: synthesis, preparation and biodistribution in rats, Journal of Controlled Release 71 (2001) 203–211.
[4] K.S. Soppimath, T.M. Aminabhavi, A.R. Kulkarni, W.E. Rudzinski, Biodegradable polymeric nanoparticles as drug delivery devices, Journal of Controlled Release 70 (2001) 1–20.
[5] S.M. Moghimi, A.C. Hunter, J.C. Murray, Long-circulating and target-specific nanoparticles: theory to practice, Pharmacological Reviews 53 (2001) 283–318.
[6] T. Govender, T. Riley, T. Ehtezazi, M.C. Garnett, S. Stolnik, L. Illum, S.S. Davis, Defining the drug incorporation properties of PLA–PEG nanoparticles, International Journal of Pharmaceutics 199 (2000) 95–110.
[7] S.K. Sahoo, J. Panyam, S. Prabha, V. Labhasetwar, Residual polyvinyl alcohol associated with poly (D, L-lactide-co-glycolide) nanoparticles affects their physical properties and cellular uptake, Journal of Controlled Release 82 (2002) 105–114.
[8] V. Nadeau, G. Leclair, S. Sant, J.-M. Rabanel, R. Quesnel, P. Hildgen, Synthesis of new versatile functionalized polyesters for biomedical applications, Polymer 46 (2005) 11263–11272.

[9] R. Quesnel, P. Hildgen, Synthesis of PLA-b-PEG multiblock copolymers for stealth drug carrier preparation, Molecules 10 (2005) 98–104.
[10] K.M. Shakesheff, C. Evora, I. Soriano, R. Langer, The adsorption of poly(vinyl alcohol) to biodegradable microparticles studied by X-ray photoelectron spectroscopy (XPS), Journal of Colloid and Interface Science 185 (1997) 538–547.
[11] G.L. Siparsky, K.J. Voorhees, J.R. Dorgan, K. Schilling, Water transport in polylactic acid (PLA), PLA/polycaprolactone copolymers, and PLA polyethylene glycol blends, Journal of Environmental Polymer Degradation 5 (1997) 125–136.
[12] C.S. Proikakis, N.J. Mamouzelos, P.A. Tarantili, A.G. Andreopoulos, Swelling and hydrolytic degradation of poly(D,L-lactic acid) in aqueous solutions, Polymer Degradation and Stability 91 (2006) 614–619.
[13] W. Abdelwahed, G. Degobert, H. Fessi, Investigation of nanocapsules stabilization by amorphous excipients during freeze-drying and storage, European Journal of Pharmaceutics and Biopharmaceutics 63 (2006) 87–94.
[14] D. Raghavan, X. Gu, T. Nguyen, M. VanLandingham, A. Karim, Mapping polymer heterogeneity using atomic force microscopy phase imaging and nanoscale indentation, Macromolecules 33 (2000) 2573–2583.
[15] S. Kopp-Marsaudon, P. Leclere, F. Dubourg, R. Lazzaroni, J.P. Aime, Quantitative measurement of the mechanical contribution to tapping-mode atomic force microscopy images of soft materials, Langmuir 16 (2000) 8432–8437.
[16] J.I. Paredes, M. Gracia, A. Martínez-Alonso, J.M.D. Tascón, Nanoscale investigation of the structural and chemical changes induced by oxidation on carbon black surfaces: a scanning probe microscopy approach, Journal of Colloid and Interface Science 288 (2005) 190–199.
[17] S.N. Magonov, V. Elings, M.H. Whangbo, Phase imaging and stiffness in tapping-mode atomic force microscopy, Surface Science 375 (1997) L385–L391.
[18] G. Donald, D. William, S. Randal, L. John, J.L. Willett, Mechanical and thermal properties of starch-filled poly(D,L-lactic acid)/poly(hydroxy ester ether) biodegradable blends, Journal of Applied Polymer Science 88 (2003) 1775–1786.
[19] H. Wang, A.B. Djurisic, W.K. Chan, M.H. Xie, Factors affecting phase and height contrast of diblock copolymer PS-b-PEO thin films in dynamic force mode atomic force microscopy, Applied Surface Science 252 (2005) 1092–1100.
[20] S.G. Wang, W.J. Cui, J.Z. Bei, Bulk and surface modifications of polylactide, Analytical and Bioanalytical Chemistry 381 (2005) 547–556.
[21] M.F. Zambaux, F. Bonneaux, R. Gref, P. Maincent, E. Dellacherie, M.J. Alonso, P. Labrude, C. Vigneron, Influence of experimental parameters on the characteristics of poly(lactic acid) nanoparticles prepared by a double emulsion method, Journal of Controlled Release 50 (1998) 31–40.
[22] A. Beletsi, Z. Panagi, K. Avgoustakis, Biodistribution properties of nanoparticles based on mixtures of PLGA with PLGA–PEG diblock copolymers, International Journal of Pharmaceutics 298 (2005) 233–241.
[23] R. Gref, M. Lück, P. Quellec, M. Marchand, E. Dellacherie, S. Harnisch, T. Blunk, R.H. Müller, 'Stealth' corona–core nanoparticles surface modified by polyethylene glycol (PEG): influences of the corona (PEG chain length and surface density) and of the core composition on phagocytic uptake and plasma protein adsorption, Colloids and Surfaces B: Biointerfaces 18 (2000) 301–313.
[24] P.D. Scholes, A.G.A. Coombes, L. Illum, S.S. Davis, J.F. Watts, C. Ustariz, M. Vert, M.C. Davies, Detection and determination of surface levels of poloxamer and PVA surfactant on biodegradable nanospheres using SSIMS and XPS, Journal of Controlled Release 59 (1999) 261–278.
[25] S. Merino, L. Brauge, A.M. Caminade, J.P. Majoral, D. Taton, Y. Gnanou, Synthesis and characterization of linear, hyperbranched, and dendrimer-like polymers constituted of the same repeating unit, Chemistry – A European Journal 7 (2001) 3095–3105.
[26] Z. Kulinski, E. Piorkowska, K. Gadzinowska, M. Stasiak, Plasticization of poly (L-lactide) with poly(propylene glycol), Biomacromolecules 7 (2006) 2128–2135.
[27] E. Piorkowska, Z. Kulinski, A. Galeski, R. Masirek, Plasticization of semicrystalline poly(L-lactide) with poly(propylene glycol), Polymer 47 (2006) 7178–7188.
[28] K.N. Shrivastava, Melting temperature, Brillouin shift, and density of states of nanocrystals, Nano Letters 2 (2002) 519–523.
[29] T. Riley, S. Stolnik, C.R. Heald, C.D. Xiong, M.C. Garnett, L. Illum, S.S. Davis, S.C. Purkiss, R.J. Barlow, P.R. Gellert, Physicochemical evaluation of nanoparticles assembled from poly(lactic acid)–poly(ethylene glycol) (PLA–PEG) block copolymers as drug delivery vehicles, Langmuir 17 (2001) 3168–3174.
[30] T. Jung, A. Breitenbach, T. Kissel, Sulfobutylated poly(vinyl alcohol)-graft-poly(lactide-co-glycolide)s facilitate the preparation of small negatively charged biodegradable nanospheres, Journal of Controlled Release 67 (2000) 157–169.
[31] F. von Burkersroda, R. Gref, A. Göpferich, Erosion of biodegradable block copolymers made of poly(-lactic acid) and poly(ethylene glycol), Biomaterials 18 (1997) 1599–1607.
[32] J.D. Clapper, J.M. Skeie, R.F. Mullins, C.A. Guymon, Development and characterization of photopolymerizable biodegradable materials from PEG–PLA–PEG block macromonomers, Polymer 48 (2007) 6554–6564.
[33] L. Youxin, C. Volland, T. Kissel, In-vitro degradation and bovine serum albumin release of the ABA triblock copolymers consisting of poly (L(+) lactic acid), or poly(L(+) lactic acid-co-glycolic acid) A-blocks attached to central polyoxyethylene B-blocks, Journal of Controlled Release 32 (1994) 121–128.
[34] B. Magenheim, M.Y. Levy, S. Benita, A new in-vitro technique for the evaluation of drug-release profile from colloidal carriers – ultrafiltration technique at low-pressure, International Journal of Pharmaceutics 94 (1993) 115–123.
[35] J. Panyam, M.M. Dali, S.K. Sahoo, W. Ma, S.S. Chakravarthi, G.L. Amidon, R.J. Levy, V. Labhasetwar, Polymer degradation and in vitro release of a model protein from poly(,-lactide-co-glycolide) nano- and microparticles, Journal of Controlled Release 92 (2003) 173–187.
[36] G. Mittal, D.K. Sahana, V. Bhardwaj, M.N.V. Ravi Kumar, Estradiol loaded PLGA nanoparticles for oral administration: effect of polymer molecular weight and copolymer composition on release behavior in vitro and in vivo, Journal of Controlled Release 119 (2007) 77–85.
[37] N. Rizkalla, C. Range, F.X. Lacasse, P. Hildgen, Effect of various formulation parameters on the properties of polymeric nanoparticles prepared by multiple emulsion method, Journal of Microencapsulation 23 (2006) 39–57.
[38] D. Sinha Roy, B.D. Rohera, Comparative evaluation of rate of hydration and matrix erosion of HEC and HPC and study of drug release from their matrices, European Journal of Pharmaceutical Sciences 16 (2002) 193–199.
[39] K.C. Sung, R.-Y. Han, O.Y.P. Hu, L.-R. Hsu, Controlled release of nalbuphine prodrugs from biodegradable polymeric matrices: influence of prodrug hydrophilicity and polymer composition, International Journal of Pharmaceutics 172 (1998) 17–25.
[40] W.N. Chen, W.J. Luo, S.G. Wang, J.Z. Bei, Synthesis and properties of poly (L-lactide)–poly (ethylene glycol) multiblock copolymers by coupling triblock copolymers, Polymers for Advanced Technologies 14 (2003) 245–253.
[41] W.J. Luo, S.M. Li, J.Z. Bei, S.G. Wang, Synthesis and characterization of poly (L-lactide)–poly(ethylene glycol) multiblock copolymers, Journal of Applied Polymer Science 84 (2002) 1729–1736.